Inorganica Chimica Acta, 86 (1984) 113–120

Studies on Mixed Metal(II)–Iron(II) Chloride Systems. Part 4. The Mössbauer and X-Ray Powder Diffraction Data for the $CsM_xFe_{1-x}Cl_3 \cdot 2H_2O$ (M = Mn, Co or Ni; x = 0, 0.5) System

BELLA Y. ENWIYA, JACK SILVER*

Department of Chemistry, University of Essex Wivenhoe Park, Colchester CO4 3SQ, Essex, U.K.

and IAN E. G. MORRISON

Department of Chemistry, Imperial College, London SW7 2AZ, U.K.

Received October 22, 1983

The octahedral Fe(II) environment containing four chlorides and two cis *water molecules is reported for the caesium materials which are demonstrated to be isostructural with* $RbM_xFe_{1-x}Cl_3 \cdot 2H_2O$ *(M = Mn, Co, Ni; x = 0, 0.5) [2]. The data for interatomic distances and hydrogen bonding in these materials are discussed in terms of the structure of* $CsMnCl_3 \cdot 2H_2O$ *from X-ray diffraction [30, 31] and* $CsFeCl_3 \cdot 2H_2O$ *from neutron diffraction [34] studies. The Mössbauer data for these compounds are reported. The chemical isomer shifts of all these materials are similar, but the quadrupole splitting data are slightly different. The data are explained in terms of changes in the site symmetry resulting in a change of orbital occupancy. The temperature dependence of the quadrupole splitting in these materials is discussed.*

Introduction

There are now Mössbauer studies of several different iron(II) chloride hydrate environments in the literature [1–27].

The crystal structures of $FeCl_2 \cdot 2H_2O$ [28] and $FeCl_2 \cdot 4H_2O$ [29] are known, and the Mössbauer data for these compounds have been explained on the basis of their structure [4, 9–12, 18–25].

In a Mössbauer spectroscopic study [1] of the $M_xFe_{1-x}Cl_2 \cdot 4H_2O$ (M = Mn, Co, Ni; x = 0–0.75) materials, we found that the quadrupole splitting decreased significantly for the Fe–Co and Fe–Ni systems. These effects were explained in terms of changes in site symmetry resulting in an alteration of orbital occupancy from $d_{xz,yz}$. The modifications in site symmetry were caused by changes in Fe–OH_2 bonding in the lattice 'squeezing' the Fe(II) centres. The Fe–Mn system also yielded results which appeared directly related to volume change but no evidence was found for pressure effects.

A study [2] of the $M'M''_xFe_{1-x}Cl_3 \cdot 2H_2O$ (M' = K, Rb; M'' = Mn, Co, Ni; x = 0, 0.5) systems yielded Mössbauer data for two different octahedral $[FeCl_4 \cdot (OH_2)_2]^{2-}$ environments. The potassium materials contained *trans*-water molecules and four chlorides in a plane, with octahedra joined in pairs sharing edges to form discrete groups $[Fe_2Cl_6 \cdot 4H_2O]^{2-}$; small differences in the quadrupole splittings between members of the group indicated that the cell size differences were mainly taken up by changes in the hydrogen bonding and potassium ion positions. The rubidium system contains *cis*-water molecules with four chlorides arranged sharing single chlorides with neighbouring octahedra in zig-zag chains. The chemical shifts of these were similar to those of the potassium group, but the quadrupole splittings were different and fall into two subsets, the pure iron and mixed manganese–iron being in one with much higher splittings and greater temperature dependence then the mixed cobalt–iron and nickel–iron materials. These differences were explained in terms of changes in site symmetry and orbital occupancy, brought about by bonding alterations caused by the different transition metal ionic radii ('pressure' effects).

To study how increase in cell size affects the quadrupole splitting we have used caesium as a cation to increase cell size. We report here the results of

*Author to whom correspondence should be addressed.

0020-1693/84/$3.00

TABLE I. The Analyses Results for $CsFe_{1/2}M_{1/2}Cl_3 \cdot 2H_2O$ (M = Mn, Fe, Co and Ni).

Compound	%Fe	%M	%Cl
$CsFeCl_3 \cdot 2H_2O$	16.9	–	32.1
	(16.86)		(32.12)
$CsFe_{1/2}Mn_{1/2}Cl_3 \cdot 2H_2O$	8.4	8.3	32.1
	(8.44)	(8.31)	(32.17)
$CsFe_{1/2}Co_{1/2}Cl_3 \cdot 2H_2O$	8.4	8.9	32.0
	(8.39)	(8.86)	(31.97)
$CsFe_{1/2}Ni_{1/2}Cl_3 \cdot 2H_2O$	8.4	8.8	32.0
	(8.40)	(8.83)	(31.98)

Calculated values in parentheses.

X-ray powder diffraction and Mössbauer spectroscopic studies of the $M'M''_xFe_{1-x}Cl_3 \cdot 2H_2O$ ($M' = Rb_yCs_z$; y = 0, 0.25, 0.5, 0.75; z = 1.0, 0.75, 0.5, 0.25; M'' = Mn, Co, Ni; x = 0, 0.5) system.

The pure $CsFeCl_3 \cdot 2H_2O$ material has been studied by other workers [26] and their interpretation has been of great use to us.

Experimental

The preparation method used for all the materials was the same, using appropriate molar ratios for the required material; for example $CsFe_{1/2}Mn_{1/2}Cl_3 \cdot 2H_2O$, 2:1:1 molar ratios of CsCl, $FeCl_2 \cdot 4H_2O$ and $MnCl_2 \cdot 4H_2O$ were used. A solution of ferrous chloride tetrahydrate is boiled with a small amount of ascorbic acid (present as reducing agent against Fe(III)), and then a solution containing the other transition metal chloride required is boiled and added to the ferrous chloride solution. The resulting solution is heated, while the alkali metal chloride solution is prepared and heated, and added to the mixed metal chloride solution. The resulting solution is evaporated to near dryness in N_2 atmosphere, and cooled in the same atmosphere.

Analytical data for $CsFe_{1/2}M_{1/2}Cl_3 \cdot 2H_2O$ materials appear in Table I. The analyses were carried out in our laboratory. The materials are very sensitive to oxidation and are handled under N_2 atmosphere.

X-ray powder diffraction data of the products were obtained using Philips 11.64 cm powder camera

TABLE II. The X-ray Powder Diffraction Data for the $CsFe_{1/2}M_{1/2}Cl_3 \cdot 2H_2O$ (M = Mn, Co and Ni) Materials.

	$CsMnCl_3 \cdot 2H_2O$			$CsFeCl_3 \cdot 2H_2O$		$Cs(Fe/Mn)Cl_3 \cdot 2H_2O$		$Cs(Fe/Co)Cl_3 \cdot 2H_2O$		$Cs(Fe/Ni)Cl_3 \cdot 2H_2O$	
I	d_{obs}	d_{cal}	*hkl*	d_{obs}	*I*	d_{obs}	*I*	d_{obs}	*I*	d_{obs}	*I*
sm	5.81	5.72	002	5.70	sm	5.75	sm	5.64	m	5.63	sm
sm	4.94	5.08	111	4.93	w	4.94	m	4.82	m	4.81	sm
sm	4.78	4.84	102	4.76	sm	4.76	m	4.70	vw	4.68	vw
vw	4.48	4.530	200	4.44	vw	4.35	s	4.41	vs	4.49	sm
vvw	4.36	4.502	012	4.27	vvw	4.32	sm	4.26	vw	4.25	vw
s	4.08	4.032	112	4.00	m	3.98	m	3.92	vs	3.90	sm
s	3.89	3.847	210	3.82	sm	3.84	m	3.74	vs	3.72	m
vvw	3.64	3.642	020	3.61	w	3.59	w	3.56	w	3.56	sm
vvw	3.20	3.193	212	3.16	w	3.20	m	3.16	sm	3.16	w
vvw	3.05	3.073	022	3.04	w	3.05	s	3.02	s	2.99	vs
vs	2.91	2.910	122	2.88	vs	2.89	vs	2.86	s	2.84	m
w	2.83	2.838	220	2.81	m	2.82	sm	2.79	vvw	2.77	vw
vvw	2.74	2.731	104	2.72	w	2.72	vw	2.71	sm	2.73	w
vs	2.67	2.671	302	2.64	vs	2.69	s	2.65	vs	2.62	vs
vvw	2.52	2.543	222	2.48	w	2.50	vw	2.48	sm	2.46	m
vvw	2.42	2.428	030	2.39	w	2.40	m	2.39	vw	2.36	vw
vvw	2.28	2.265	400	2.26	vw	2.27	vw	2.23	w	2.23	w
vvw	2.24	2.235	032	2.22	vvw	2.22	vvw	2.16	m	2.15	m
s	2.03	2.023	412	2.015	s	2.02	s	2.01	m	2.01	w
s	2.01	1.998	314	1.985	s	1.994	s	1.983	sm	1.979	m
vw	1.996	1.999	133	1.961	w	1.959	m	1.959	m	1.957	w
sm	1.933	1.923	420	1.909	sm	1.918	w	1.899	vw	1.897	vw
sm	1.911	1.909	006	1.883	vw	1.897	m	1.879	w	1.875	w
vw	1.877	1.868	106	1.861	vw	1.870	vw	1.847	vw	1.845	vw
vvw	1.852	1.852	034	1.826	vw	1.845	w	1.814	vw	1.814	w
vvw	1.801	1.809	116	1.796	w	1.801	vw	1.791	w	1.786	vw
vw	1.757	1.759	206	1.745	w	1.742	vw	1.742	w	1.739	w
vw	1.714	1.714	234	1.697	vvw	1.706	vvw	1.684	vvw	1.682	vvw
vw	1.700	1.705	142	1.671	vvw	1.687	vvw	1.663	vvw	1.661	vvw

TABLE III. Cell Sizes for the $CsFe_{1/2}M_{1/2}Cl_3 \cdot 2H_2O$ (M = Fe, Mn, Co, Ni) Materials, All Materials are Orthorhombic.

Compound	*a*/Å	*b*/Å	*c*/Å
$CsMnCl_3 \cdot 2H_2O$[a]	9.060(5)	7.285(5)	11.455(5)
$CsFeCl_3 \cdot 2H_2O$	8.98(1)	7.21(1)	11.38(1)
$CsFe_{1/2}Mn_{1/2}Cl_3 \cdot 2H_2O$	9.02(1)	7.25(1)	11.42(1)
$CsFe_{1/2}Co_{1/2}Cl_3 \cdot 2H_2O$	8.95(1)	7.09(1)	11.29(1)
$CsFe_{1/2}Ni_{1/2}Cl_3 \cdot 2H_2O$	8.94(1)	7.06(1)	11.27(1)

[a]Values from ref. [30].

and Cu–K_α radiation. The X-ray powder diffraction data appears in Table II.

The Mössbauer apparatus has been described previously [2]. The source was 6 mCi ^{57}Co–Cu. The solid absorbers were finely powdered and sealed in perspex holders with 'sellotape'; the absorber thickness was 0.01 ~ 0.02 g cm^{-2}. Velocity calibrations were carried out using thin 10 mg cm^{-2} high purity iron foils. The spectra were analysed by a simple non-linear least-squares fitting program; all chemical isomer shifts are referred to natural iron.

Results and Discussion

Structure of $CsM_xFe_{1-x}Cl_3 \cdot 2H_2O$ (M = Mn, Co, Ni)

The detailed X-ray powder diffraction data (supplementary data) show that all the materials are isostructural with α-$RbMnCl_3 \cdot 2H_2O$ and $CsMnCl_3 \cdot 2H_2O$; they all show sharp lines, suggesting that they are distinct phases and not mixtures of the parent compounds.

Cell sizes are given in Table III. The major bond lengths, calculated from these cell sizes and assuming the atom coordinates are those of $CsMnCl_3 \cdot 2H_2O$ [30] are shown in Table IV.

Crystal Structure of $CsMnCl_3 \cdot 2H_2O$ [30]

This compound is known to crystallise in the orthorhombic space group Pcca with four formula units per unit cell; this structure is also observed in α-$RbMnCl_3 \cdot 2H_2O$ [31] (Fig. 1). The manganese atom is octahedrally coordinated to four chlorine atoms and two water molecules, the latter occupying *cis*-positions, and the octahedra form infinite zigzag chains by corner sharing at a chlorine (Cl_I). Neighbouring chains have a weak coupling in the *c*-direction by hydrogen bonding between the water molecules of one chain and the non-bridging chlorines (Cl_{II}) of the other, and the planes formed in this way are separated in the *b*-direction by planes of caesium cations.

TABLE IV. The Major Bond Lengths Found in the $CsFe_{1/2}M_{1/2}Cl_3 \cdot 2H_2O$ (M = Fe, Mn, Co, Ni) Compared to Those Found in the Parent $CsMnCl_3 \cdot 2H_2O$.

	$CsMnCl_3 \cdot 2H_2O$[a]	$CsFeCl_3 \cdot 2H_2O$	$CsFe_{1/2}M_{1/2}Cl_3 \cdot 2H_2O$	$CsFe_{1/2}Co_{1/2}Cl_3 \cdot 2H_2O$	$CsFe_{1/2}Ni_{1/2}Cl_3 \cdot 2H_2O$
within octahedra					
M–Cl(I)	2.57	2.53	2.54(2)	2.52(2)	2.52(2)
M–Cl(II)	2.50	2.46(2)	2.47(2)	2.43(2)	2.43(2)
M–O	2.08	2.04(2)	2.05(2)	2.02(2)	2.01(2)
between neighbouring octahedra					
Cl(I)–Cl(II)	3.83	3.78(1)	3.81(1)	3.76(1)	3.76(1)
Cl(II)–O (h)	3.14	3.11(1)	3.12(1)	3.10(1)	3.10(1)
Cl(II)–O (h)	3.30	3.26(1)	3.28(1)	3.24(1)	3.24(1)

[a]These data are taken from ref. [30].

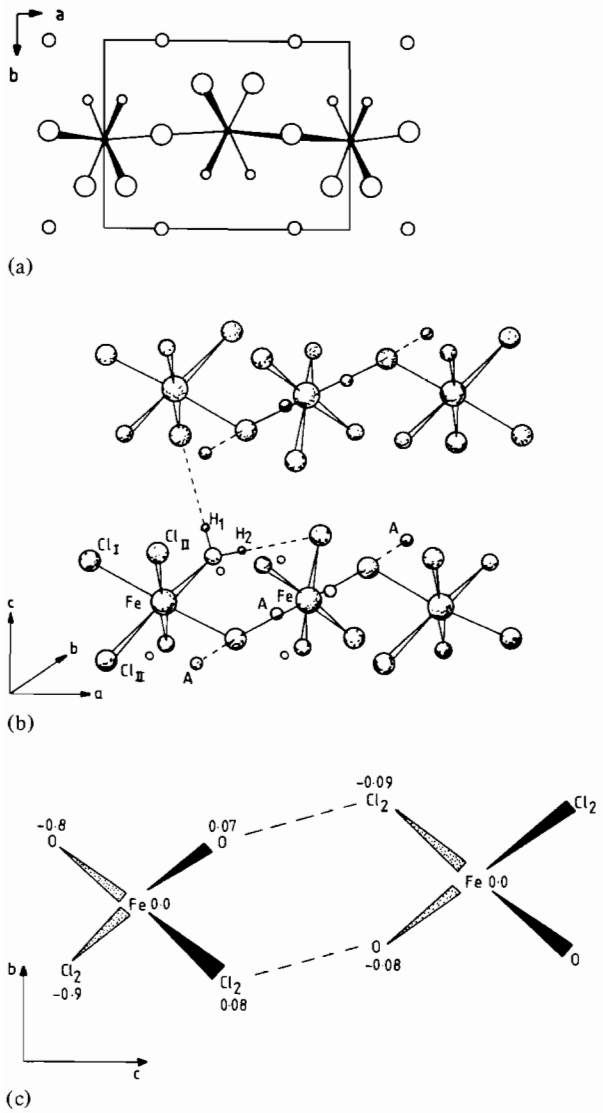

Fig. 1. Structure of $CsMnCl_3 \cdot 2H_2O$. (a) Projection of half-unit cell on (001). (b) Schematic representation of structure; only one set of hydrogen bonds is shown. (c) Projection showing hydrogen bonds in bc plane; numbers indicate distance of the atom above or below this plane, and dashed line indicates interchain hydrogen bonds. (Note: this corrects the earlier misrepresentation of the H-bonds in ref. [2], page 1043).

$CsCoCl_3 \cdot 2H_2O$ has been examined by X-ray powder diffraction [32] and the deuterated form by neutron diffraction [33] and found to have the same structure. Neutron diffraction powder data for $CsFeCl_3 \cdot 2D_2O$ [26, 34, 35] has indicated an isostructural material with some minor differences in the atomic coordination. Evidence for the hydrogen bonding network in all these compounds can be traced to the original $CsMnCl_3 \cdot 2H_2O$ and α-$RbMnCl_3 \cdot 2H_2O$ structures [30, 31, 36]. In fact, succeeding workers in this field [32–35, 37] all base their hydrogen or deuterium atom positions on this work. In line with all others we are assuming that this hypothesis is correct and the H-bonding network lies predominantly in the ca plane (Fig. 1) with one O–H···Cl(II) bond being within the chain and the other between two adjacent chains. The result of these hydrogen bonds lying in the ca plane is said to be the easy cleavage parallel to the ab plane [38].

For the work reported here we have performed calculations on the pure iron complexes using atomic coordinates from (a) single crystal X-ray diffraction data on $RbMnCl_3 \cdot 2H_2O$ and $CsMnCl_3 \cdot 2H_2O$ [30, 31] and (b) neutron diffraction data for $CsFeCl_3 \cdot 2D_2O$ [34]; the results of these calculations are given in Table V and are not consistent. The atomic coordinates from (b) we judge to be less precise as

(1) the authors state they had to allow for preferred orientation [34];

(2) these were based on powder data, which are less extensive in data base than the single crystal X-ray data on which the Mn results were based [30, 31];

(3) the neutron diffraction data for the Fe materials were themselves based on a similar fit for $CsCoCl_3 \cdot 2D_2O$ at 100 K [33].

From Table III it is obvious that the bond lengths decrease in the order $Mn > Mn_{1/2}Fe_{1/2} > Fe > Fe_{1/2}Co_{1/2} > Fe_{1/2}Ni_{1/2}$. The surprising results are not in this data but are found in comparing that of $RbFeCl_3 \cdot 2H_2O$ to $CsFeCl_3 \cdot 2H_2O$ (Table V); these octahedra are quite different. In the presence of the larger cation the Fe–O and Fe–Cl(II) bond lengths are shorter and the bridging Fe–Cl(I) is longer. The Fe–Fe distance also increases. All the Cs contacts are longer than the corresponding Rb lengths, as would be expected under the conditions assumed with the increase in cell size. This change must be due primarily to the presence of the larger Cs ions separating the chains of the octahedra, and is also manifest in the larger change in the unit cell size in the *b*-direction in the Cs materials. The effect of the hydrogen bonds will reinforce this, as they link the chains in the *c*-direction, and also are between the oxygen and Cl(II) atoms within the chains principally along the *a*-axis; thus the least restraining force will be in the *b*-direction. The secondary effect of these larger Cs ions must be to weaken the hydrogen bonding between the chains (Table V) and this is manifest by shorter Fe–O bond lengths, and an increase in the length of the chlorine bridge bond, and an increase in the length of the hydrogen bond from Cl(II)–O between the chains. The intra-chain hydrogen bond length in fact decreases slightly and the Fe–Cl(I)–Fe angle decreases.

TABLE V. The Major Bond Lengths Found in the $AFeCl_3 \cdot 2H_2O$ (A = Rb, Cs) and $CsFe_{1/2}Mn_{1/2}Cl_3 \cdot 2H_2O$, in Accordance to the Atomic Position Represented in ref. [35], Using the Cell Sizes Presented in this work.

	$RbFeCl_3 \cdot 2H_2O$	$CsFeCl_3 \cdot 2H_2O$	$CsFe_{1/2}Mn_{1/2}Cl_3 \cdot 2H_2O$
within octahedra			
M–O	2.149	2.058	2.067
M–Cl(I)	2.533	2.550	2.560
M–Cl(II)	2.503	2.476	2.486
M–M	4.505	4.516	4.536
M–Cl(I)–M	125.5	124.6	124.7
Cl(I)–M–O	86.6	84.9	84.9
Cl(II)–M–O	91.0	89.3	89.4
Cl(II)–M–Cl(I)	95.4	95.4	95.4
Cl(I)–M–Cl(I)	167.4	169.3	169.3
between octahedra			
Cl(I)–O	3.699	3.788	3.801
Cl(II)–O	3.647	4.047	4.067
Cl(II)–O (h) within	3.157	3.118	3.132
Cl(II)–O (h) between	3.168	3.274	3.286
Cs/Rb–Cl(I)	3.480	3.607	3.625
Cs/Rb–Cl(II)	3.399	3.561	3.574
Cs/Rb–Cl(II)	3.545	3.651	3.664
Cs/Rb–Cl(II)	3.341	3.455	3.470
Cs/Rb–O	3.719	3.745	3.760
Cs/Rb–O	3.664	3.807	3.824
Cs/Rb–M	4.073	4.218	4.238
Cs/Rb–Cs/Rb	5.036	5.077	5.098

TABLE VI. ^{57}Fe Mössbauer Data for the $CsFe_{1/2}M_{1/2}Cl_3 \cdot 2H_2O$ (M = Fe, Mn, Co, Ni).

Compound		T/K	δ/mm sec^{-1}	Δ/mm sec^{-1}	Γ/mm sec^{-1}
$CsFeCl_3 \cdot 2H_2O$	I[a]	298	1.163(2)	1.380(4)	0.123(3)
		80	1.290(2)	1.443(4)	0.118(3)
	II[a]	80	1.288(2)	1.441(4)	0.117(3)
		180	1.234(2)	1.425(5)	0.118(4)
		260	1.178(3)	1.397(5)	0.123(5)
		298	1.162(3)	1.377(6)	0.127(5)
$CsFe_{1/2}Mn_{1/2}Cl_3 \cdot 2H_2O$		80	1.292(3)	1.410(6)	0.108(5)
		180	1.237(4)	1.397(9)	0.118(7)
		298	1.157(3)	1.360(6)	0.120(5)
$CsFe_{1/2}Co_{1/2}Cl_3 \cdot 2H_2O$		80	1.289(4)	1.483(8)	0.119(6)
		180	1.230(4)	1.446(9)	0.121(8)
		298	1.166(7)	1.366(14)	0.127(12)
$CsFe_{1/2}Ni_{1/2}Cl_3 \cdot 2H_2O$		80	1.282(5)	1.514(9)	0.132(8)
		180	1.206(6)	1.448(12)	0.146(10)
		298	1.154(6)	1.385(12)	0.132(10)

[a]Two different $CsFeCl_3 \cdot 2H_2O$ samples were prepared. Their data are included here for comparison.

The hydrogen bonding between the chains is important in the packing (and/or squeezing) as suggested in the parent $CsMnCl_3 \cdot 2H_2O$ [30]. These hydrogen bonds change as one transition metal is substituted for another (Table IV); the *a*-direction shows most evidence of squeezing the Fe(II) ion and

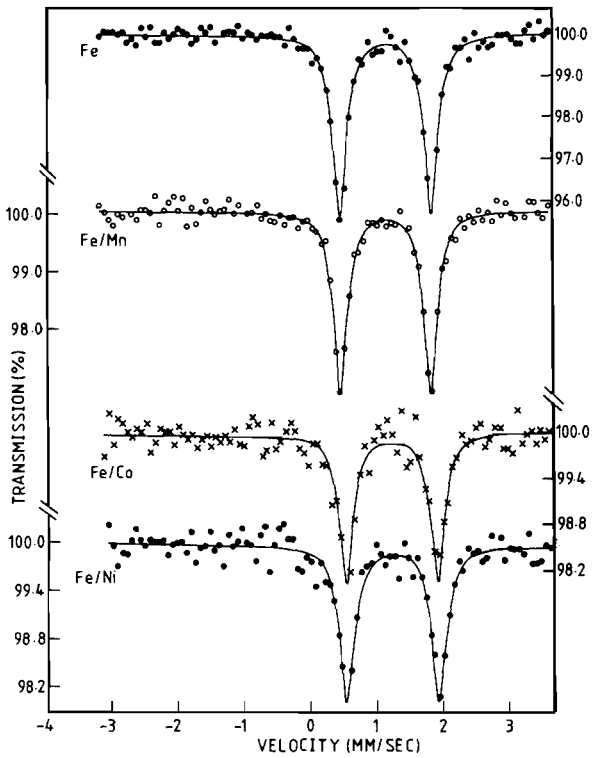

Fig. 2. Mössbauer spectra at room temperature for materials $CsFe_{1/2}Me_{1/2}Cl_3 \cdot 2H_2O$ (M = Mn, Fe, Co, Ni).

this will experience changes in the crystal field splitting resulting from this applied pressure.

In the $CsFe_{1/2}M_{1/2}Cl_3 \cdot 2H_2O$ (M = Co and Ni) materials, the Co(II) and Ni(II) ions are both smaller than Fe(II) and thus Fe(II) is squeezed by them in the *a*-direction along the chains; this should split any remaining degeneracy of the t_{2g} levels.

For the $CsFe_{1/2}Mn_{1/2}Cl_3 \cdot 2H_2O$ compound, the manganese ions are larger than the Fe(II) and the unit cell is larger than that of $CsFeCl_3 \cdot 2H_2O$. Therefore the Fe(II) ions are now less constrained and the result should be more symmetrical iron electronic environments; this should result in a smaller crystal field splitting of the d-orbitals.

Mössbauer Discussion

The Mössbauer spectroscopic data (Table VI and Fig. 2) for the materials $CsFe_{1/2}M_{1/2}Cl_3 \cdot 2H_2O$ (M = Mn, Co, Ni) are very similar to those of $CsFeCl_3 \cdot 2H_2O$. All the materials in this series have a small quadrupole splitting similar to that of $RbFe_{1/2}Mn_{1/2}Cl_3 \cdot 2H_2O$ [2].

At 80 K the quadrupole splittings for $CsFe_{1/2}M_{1/2}Cl_3 \cdot 2H_2O$ (M = Mn, Fe, Co, Ni) are in the order Ni > Co > Fe > Mn. This order remains the same at 180 K, but at 300 K the range of splittings is smaller (1.36 ~ 1.39 mm sec^{-1} compared with 1.41 ~ 1.51 mm sec^{-1} at 80 K) and the order of Co and Ni is less distinct.

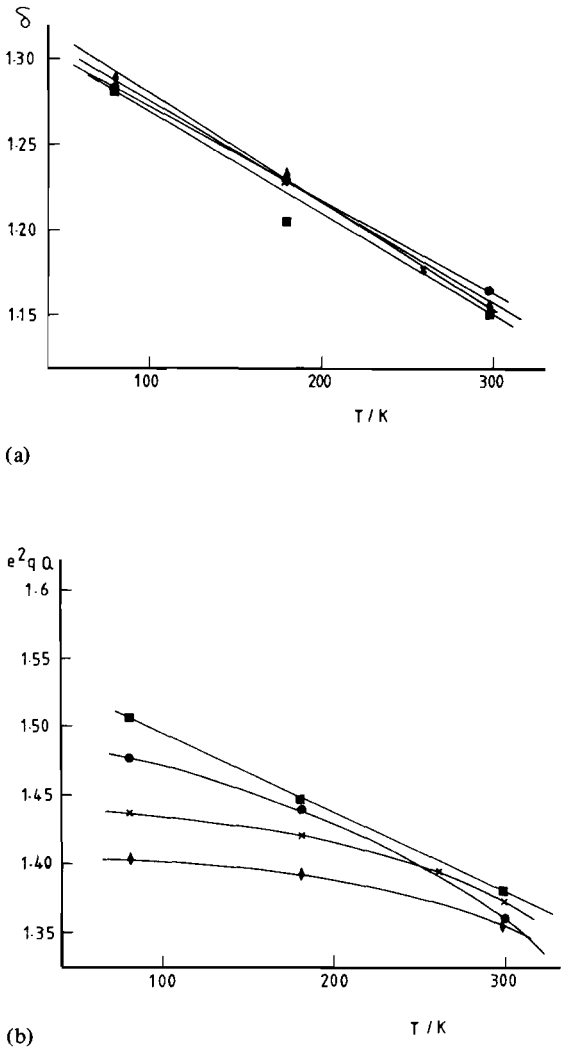

Fig. 3. Mössbauer parameters as a function of temperature for $CsFe_{1/2}M_{1/2}Cl_3 \cdot 2H_2O$ (M = Mn, Fe, Co, Ni). (a) Isomer shift. (b) Quadrupole splitting. × $CsFeCl_3 \cdot 2H_2O$; ♦ Mn/Fe; • Fe/Co; ▪ Fe/Ni.

The isomer shifts for all these materials are very similar both at 80 K and 298 K (Fig. 3(a)), although (allowing for errors) there is some indication that the nickel compound has the smallest shift. These caesium materials have isomer shifts that are very similar to those for the Rb materials reported previously [2], as may be expected from the fact that these distant cations would not contribute to the 4s electron density. The nearly identical isomer shifts indicate that the materials have Fe(II) environments with similar 'p' and 'd' electron participation in the bonding.

The changes in the isomer shifts, though slight, are in accordance with Drickamer's work [39]; when the pressure is applied at the iron nucleus (*i.e.* an increase in the s-electron density) when the isomer shifts will decrease; this would be consistent with a reduction in 3d shielding.

In accordance with Drickamer's pressure experiments, an increase of the quadrupole splitting would be expected, but as stated therein this is not found for FeF_2 or $FeSO_4 \cdot 7H_2O$, and interpretation requires detailed knowledge of local symmetry changes, spin–orbit coupling factors as well as local compressibility. In our linear chain materials there is a slight increase in splitting with pressure (Fig. 3b).

The quadrupole splittings found in the caesium materials must be compared with those previously reported for the rubidium series [2]. The $RbFeCl_3 \cdot 2H_2O$ and $RbFe_{1/2}Mn_{1/2}Cl_3 \cdot 2H_2O$ materials have the larger cell sizes and in these the iron(II) ions are not squeezed; whereas the reverse is true for the $RbFe_{1/2}M_{1/2}Cl_3 \cdot 2H_2O$ (M = Co, Ni). In this report, in the $CsFe_{1/2}M_{1/2}Cl_3 \cdot 2H_2O$ (M = Mn, Fe, Co, Ni) we have a similar effect but modified by the presence of the large Cs cation. The expansion in the cell size caused by this cation produces the smaller quadrupole splitting values, compared with $RbFeCl_3 \cdot 2H_2O$, resulting from the increase in M–Cl(I) bridging bond lengths and shorter M–O and M–Cl(II) lengths. Within the $CsFe_{1/2}M_{1/2}Cl_3 \cdot 2H_2O$ series, the closest approach to the rubidium splitting is found with nickel which will oppose the effect of caesium, and the greatest departure from the rubidium splitting is obtained with manganese, which should reinforce the larger cation in allowing the iron the opportunity for the most symmetrical environment in these materials.

All the caesium materials show only small temperature dependence of the quadrupole splitting. There are two possible ways this behaviour could arise:

(a) A singlet ground state with a very large energy gap to the first excited level (to give temperature independence), with a lattice contribution of opposite sign.

(b) A doublet ground state (brought about by atomic readjustment of the Fe(II) in the larger holes causing an inversion of the tetragonal field). A similar inversion was found in $M_xFe_{1-x}Cl_2 \cdot 4H_2O$ (M = Co, Ni) [1].

Although (b) would be expected to give rise to a lower quadrupole splitting than found here, the lower than tetragonal symmetry may split the ground state slightly, combined with an altered lattice contribution over the temperature range arising from small changes in atomic position, such as that reported for the D_2O in $RbFeCl_3 \cdot 2D_2O$ and $CsFeCl_3 \cdot 2D_2O$ [35].

TABLE VII. The Calculated Bond Lengths (Å) around the Iron Atoms for $RbFeCl_3 \cdot 2D_2O$ and $CsFeCl_3 \cdot 2D_2O$ Using Atomic Data and Cell Sizes Presented in ref. [35].

	$RbFeCl_3 \cdot 2D_2O$		$CsFeCl_3 \cdot 2D_2O$	
	77 K	4.2 K	300 K	4.2 K
bonds				
Fe–O	2.16	2.16	2.13	2.12
Fe–Cl(I)	2.50	2.51	2.52	2.51
Fe–Cl(II)	2.43	2.47	2.49	2.47
angles				
Cl(I)–Fe–O	86.1	86.5	87.5	87.9
Cl(II)–Fe–O	91.3	91.8	92.1	90.4
Cl(II)–Fe–Cl(I)	94.1	94.5	93.3	93.5

Detailed analyses of the quadrupole splitting data for $RbFeCl_3 \cdot 2H_2O$ have been reported [26] and analysed in terms of both (a) and (b); although explanation (a) could give rise to the observed maximum value of ~1.48 mm sec^{-1} at 110 K, the sign and magnitude of V_{zz} (valence) did not agree with their other experimental data. The data above 120 K was consistent with (b), but the data below this could only be explained by onset of magnetic short-range interactions. This analysis is also applied to the caesium compound $CsFeCl_3 \cdot 2H_2O$ [26].

The differences in quadrupole splitting between the Cs and Rb pure iron materials are as stated related to the presence of the Cs^+ cation causing lattice expansion. However if the atomic positions given by Basten *et al.* [35] are assumed correct along with the cell sizes quoted then there is a large change in crystallographic environments around the iron positions (Table VII). These changes are mainly in the Fe–O bond lengths but they are only manifest as slight changes in the Mössbauer parameters. The explanation for this is that either the electronic environments around the iron atoms in these materials are very similar and do not reflect the crystallographic environment or that the atomic positions given in reference 35 are not correct for the corresponding hydrogen materials.

The hydrogen bonds between the octahedral chains are very important in packing the octahedra, as has been suggested in $CsMnCl_3 \cdot 2H_2O$ [30, 40] and the analogous materials [32]. These hydrogen bonds change length when different transition metals are substituted in the lattice (Table IV). There is no strong evidence from the Mössbauer data as to whether these hydrogen bonds affect the electronic environments directly.

The electric field gradient tensor has a contribution from charges external to the central atom, the

'lattice' term; slight changes in this could account for small differences in quadrupole splitting values. Such changes could in principle arise from the different electron populations in nearby transition metal ions; but these would be very small. A larger change would be expected if the octahedral size altered; but since there is no such change in these materials, the lattice effect will be neglected.

Conclusions

From this work it is apparent that the larger Cs^+ ions cause the chains to be further apart as seen in Table V for the hydrogen bond distances between the chains. The changes in quadrupole splitting for the Cs compounds compared to the Rb materials [2] reflects the changes in cell size.

References

1 B. Y. Enwiya, J. Silver and I. E. G. Morrison, *J. Chem. Soc. Dalton Trans.*, 2231 (1982).
2 B. Y. Enwiya, J. Silver and I. E. G. Morrison, *J. Chem. Soc. Dalton Trans.*, 1039 (1983).
3 R. W. Grant, H. Wiederish, A. H. Muir, U. Gonser and W. N. Delgass, *J. Chem. Phys., 45,* 1015 (1966).
4 K. Ono, M. Shinohara, A. Ito, T. Fujita and A. Ishigaki, *J. Appl. Phys., 39,* 1126 (1968).
5 C. D. Burbridge and D. M. L. Goodgame, *J. Chem. Soc. A.*, 1410 (1968).
6 A. J. Nozik and M. Kaplan, *J. Chem. Phys., 47,* 2960 (1967).
7 J. V. Dilorenzo and M. Kaplan, *J. Chem. Phys. Lett., 3,* 216 (1969).
8 C. E. Johnson and M. S. Ridout, *J. Appl. Phys., 38,* 1272 (1967).
9 P. Zory, *Phys. Rev., 140,* A1401 (1965).
10 A. J. Nozik and M. Kaplan, *Phys. Rev., 159,* 273 (1967).
11 S. Chandra and G. R. Hoy, *Phys. Lett., 22,* 254 (1966).
12 C. E. Johnson, *Proc. Phys. Soc., London, 88,* 943 (1966).
13 G. Ziebrath, *Z. Phys., 212,* 330 (1968).
14 A. Vertes, T. Szekely and T. Tarnoczy, *Acta Chm. Acad. Sci. Hung., 63,* 1 (1970).
15 A. Vertes, *Acta Chim. Acad. Sci. Hung., 3,* 1 (1970).
16 G. A. Sawatzky and Van Der Woude, *Chem. Phys. Lett., 4,* 335 (1969).
17 B. Brunot, *J. Chem. Phys., 6,* 2360 (1974).
18 T. C. Gibb, *Chem. Phys., 7,* 449 (1975).
19 M. Shinohara, *J. Phys. Soc. Jpn., 42,* 65 (1977).
20 W. Siebke, S. Hosl, H. Spiering and G. Ritter, Proc. Conf. Mössbauer Spectroscopy, Bratislava, p. 176 (1973).
21 H. Spiering, S. Hosl and H. Vogel, *Phys. Status Solidi B, 85,* 87 (1978).
22 H. Spiering and H. Vogel, *Hyperfine Interact., 3,* 221 (1977).
23 R. Zimmermann, *Nucl. Instrum. Methods, 128,* 537 (1975).
24 I. O. Suzdalev and A. P. Amulyavichus, *Zh. Exsp. Teor. Fiz., 61,* 2354 (1971).
25 J. Tatarkiewez, *Postepy. Fiz., 26,* 641 (1976).
26 H. Th. Le Fever, R. C. Thiel, W. J. Huiskamp and W. J. M. de Jonge, *Physica B, 111,* 190 (1981).
27 H. Th. Le Fever, R. C. Thiel, W. J. Huiskamp, W. J. M. de Jonge and A. M. Van Der Kraan, *Physica B, 111,* 209 (1981).
28 B. Morosin and E. J. Graeber, *J. Chem. Phys., 42,* 898 (1965).
29 B. R. Penfold and J. A. Grigor, *Acta Cryst., 12,* 850 (1959).
30 S. J. Jensen, P. Andersen and S. E.Rasmussen, *Acta Chem. Scand., 16,* 1890 (1962).
31 S. J. Jensen, *Acta Chem. Scand., 21,* 889 (1967).
32 N. Thorup and H. Soling, *Acta Chem. Scand., 23,* 2933 (1969).
33 A. L. M. Bongaarts, *Ph.D. Thesis,* Ract. Cent. Nederland, Petten, Neth., RCN-Rep, RCN-235, pp. 139 (1975).
34 Q. A. G. Van Vlimmeren, C. H. W. Swüste and W. J. M. de Jonge, *J. De Physique Colloque, C6, 39,* 743 (1978).
35 J. A. J. Basten, Q. A. G. Van Vlimmeren and W. J. M. de Jonge, *Phys. Rev., B, 18,* 2179 (1978).
36 S. J. Jensen, 'Hydrater of Nogle Divalente Metallers Chlorides Diss.', p. 76 (1969).
37 Z. M. El Saffar, *J. Chem. Phys., 52,* 4097 (1970).
38 A. Herweijer, W. J. M. de Jonge, A. C. Botterman, A. L. M. Bongaarts and J. A. Cowen, *Phys. Rev. B, 5,* 4618 (1972).
39 A. R. Champion, R. W. Vaughan and H. G. Drickamer, *J. Chem. Phys., 47,* 2583 (1967).
40 H. Bug, H. Haas, M. Fleissner and H. Harlmann, *J. Chem. Phys., 55,* 280 (1971).